Study of stellar populations in the bulges of barred galaxies[⋆]

I. Pérez[1,2] and P. Sánchez-Blázquez[3,4,5,6]

[1] Dep. Física Teórica y del Cosmos, Campus de Fuentenueva, Universidad de Granada, E-18071 Granada, Spain
  e-mail: isa@ugr.es
[2] Instituto Carlos I de Física Teórica y Computación, Spain
[3] Dep. Física Teórica, Universidad Autonoma de Madrid, Cantoblanco, E-28049, Madrid, Spain
[4] Instituto de Astrofísica de Canarias, c/Vía Láctea s/n, E-38200, La Laguna, Tenerife, Spain
[5] Departamento de Astrofísica, Universidad de La Laguna, E-38205 La Laguna, Tenerife, Spain
[6] Jeremiah Horrocks Institute, UCLan, Preston, PR1 2HE, UK
  e-mail: :p.sanchezblazquez@uam.es

ABSTRACT

Aims. To determine the influence of bars in the building of galaxy bulges through the analysis of ages and metallicities derived from stellar absorption line-strength indices.

Methods. Long-slit spectroscopy was obtained for a sample 20 early-type barred galaxies. Line strength indices were measured and used to derive age and metallicity gradients in the bulge region by comparing with stellar population models. The same analysis was carried out with similar data of unbarred galaxies taken from the literature.

Results. The bulges of barred galaxies seem to be more metal rich, at a given velocity dispersion (σ), than the bulges of unbarred galaxies, as measured by some metallicity sensitive indices. There are indications that the ratio of relative abundance of alpha-elements with respect to iron, [E/Fe], derived for the bulges of barred galaxies tend to lie above the values of the unbarred galaxies at a given σ. The metallicity gradients for the majority of the bulges are negative, less metal rich towards the end of the bulge. The gradient values show a large scatter for galaxies with σ below 150 km s^{-1}. The age distribution is related to the presence of bulge substructure such as a nuclear ring or an inner disk. The metallicity of both the bulge and the bar are very well correlated indicating a close link between the enrichment histories of both components.

Conclusions. Bulges of barred early type galaxies might have suffered a different chemical enrichment compared to the bulges of unbarred galaxies of the same morphological type, same central velocity dispersion and low inclination angles. The hinted stellar populations differences separating the bulges of barred and unbarred galaxies and the strong link existing between the metallicity of the bulge and the presence of a bar points to scenarios were they both form simultaneously in processes leading to rapid and massive episodes of star formation, possibly linked to the bar formation. In order to confirm and generalise the results found here, it would be useful to extend the data set to a larger number of unbarred galaxies and a wider range of morphological types

Key words. Galaxies: abundances – Galaxies:bulges – Galaxies: structure – Galaxies: stellar content – Galaxies:evolution

1. Introduction

If we consider that galaxy bulges of disk galaxies are the excess of light from the exponential disk, excluding the bar (e.g. Freeman 1970; Fisher 2006; Peletier 2008), we can find two types of bulges. In the standard picture, the two types of bulges are separated between those formed through violent processes ('classical bulges') and those formed slowly through internal processes (i.e., through secular evolution) (e.g. Simkin et al. 1980; Pfenniger & Friedli 1991; Hopkins et al. 2010) They are expected to have very different structural properties; the bulges formed via secular evolutionary processes are expected to have more disk–like properties while the so called 'classical' bulges are expected to have properties more related to elliptical galaxies (e.g. Fisher & Drory 2008; Gadotti 2009; Fisher & Drory 2010, for a detail discussion on the properties on both types of bulges, see the review by Kormendy & Kennicutt 2004 and references therein). However, both bulges can coexist and the observed properties sometimes depend on the geometry chosen to derive the bulge properties.

Much work has been done trying to characterise the influence of the disk in the bulge evolution by comparing the stellar populations of bulges and those of elliptical galaxies and, up to date, there is not consensus in the final conclusions. Some authors (e.g. Thomas & Davies 2006; Goudfrooij, Gorgas & Jablonka 1999) have concluded that, galaxies with morphological types from E to as late as Sbc, have stellar population properties that are correlated to the central velocity dispersion (σ) and that, at a given σ, bulges and elliptical galaxies cannot be distinguished as far as their stellar populations are concerned, indicating very little influence of the disc in the evolution of the bulge. Recent work by MacArthur, Gonzalez & Courteau (2009) derived the whole star formation histories for the bulges of a sample of eight galaxies, finding that the mass weighted stellar ages of the bulges are old and that, therefore, secular evolution effects only contribute minimally to the total bulge mass.

However, other authors (e.g.Falcón-Barroso et al. 2002; Peletier et al. 2007; Ganda et al. 2007) find that the Mg–σ relation for the bulges lies below that found for elliptical galaxies. Proctor & Sansom 2002 go further concluding that the stel-

lar population trends greatly differ between early and late type galaxies.

Part of the discrepancy between different studies can be due to the selection of the sample. For example, inclination effects can make the contribution to the integrated spectra of the different galaxy components appear larger or smaller depending on the inclination (see Peletier et al. 2007). Furthermore, the morphological selection and the range in luminosities chosen might bias the conclusions as kinematical studies indicate that secularly formed bulges are more important in late type spirals and especially in low-luminous ones.

An alternative way to determine the influence of secular evolution in the growing of bulges is to compare similar spiral galaxies (in terms of luminosity, morphology and inclination) with and without bars. Bars are expected to play an important role in the secular evolution of disk galaxies and they are obvious candidates to produce secular evolution and create a bulge secularly in disk galaxies. The bar gravity torques make the gas lose angular momentum which, in turn, provokes an inflow of gas towards the central parts (e.g. Pfenniger & Norman 1990; Combes et al. 1990; Friedli & Benz 1995). Star formation might be triggered and, possibly, the formation of a stellar bulge. One obvious way to study the efficiency of this process is to compare the star formation history of bulges in galaxies with and without bars. These type of studies have to be done in face-on galaxies where it is easy to morphologically identify the bar. There have been only a handful of studies characterising the bulges from samples of face-on galaxies. 39 galaxies were analysed by Moorthy & Holtzman (2006) . From these, 19 have low inclination, and eleven are barred. They found that bars have smaller Hβ (indicating older luminosity-weighted ages) that unbarred galaxies at a fixed central velocity dispersion and maximum rotational velocity. They also analysed the distribution of the stellar populations with radius, finding that, when positive age gradients exists, they were always found in barred galaxies. On the contrary, studies focused only on edge-on galaxies attempting to classify bars such as Jablonka et al. (2007) do not find any difference between the indices in barred and unbarred galaxies, neither in the central values nor in the gradients.

We have started a project to characterise the stellar properties of barred galaxies to understand the influence of bars in the evolution of the different galaxy components and to study their formation. In Pérez, Sánchez-Blázquez & Zurita (2007) and Pérez, Sánchez-Blázquez & Zurita (2009, hereafter, Paper I), we presented a detailed analysis of the stellar population parameters along the bar of a sample of 20 galaxies. From the results obtained (kinematics and SSP derived stellar population parameters along the bar) we determined that the bulge kinematics is closely linked to the presence of a bar. Some studies, however, have not found any correlation between the presence of a bar and the bulge properties, probably due to an inclination bias because studies of more inclined objects will avoid the contribution of the inner disc–like components. To conclude whether bars have a strong influence in the properties of bulges, a systematic comparison of bulges of barred and unbarred galaxies needs to be done, using galaxies with similar inclination, morphological type and central velocity dispersion. We present, in this paper, the study of the stellar population properties of the central regions of the 20 barred galaxies analysed in Paper I. For an analysis of the differences between the bulges of barred and unbarred galaxies our sample would need to be complemented with a similar sample of galaxies without bars. So, in addition to the bulges of barred galaxies, we present, in this paper, a comparison with Moorthy et al. (2006) data from a sample of both, barred and unbarred

galaxies, being the only sample available in the literature with similar characteristics to our data; namely, spectral coverage and resolution, morphological type and inclination values. The data have been re–analysed in the same way as for our sample. This is the first time that such study is done for a large sample of barred galaxies, with a total of 31 barred galaxies combining both samples. Due to the low number of unbarred galaxies compared to the barred galaxies in the total sample, we will extend the sample in the future to include a larger number of unbarred galaxies and to cover a wider range in morphological types.

In Secs. 2, 3 and 4 we give a brief introduction to the sample selection, observations and, data reduction and line-strength measurements. A more detailed explanation of these sections is given in Paper I. An analysis of the central line–strength indices and a comparison between barred and unbarred galaxies is given in Sect. 5.1. The line–strength index distributions in the bulge region are presented in Sect. 5.3. The single stellar population equivalent parameters are discussed in Section 6. The age and metallicity gradients are presented in Section 6.1, while a comparison between the stellar parameters in the bulge and bar region is given in Sect. 6.2. The conclusions and discussion are presented in Sect. 7.

2. Sample characterisation

We have selected barred galaxies from the Third Reference Catalogue of bright galaxies (RC3) (de Vaucouleurs 1948) with the following criteria; to be classified as barred, with inclinations between $10°$ and $70°$, and nearby ($cz \leq 4000 \, \mathrm{kms}^{-1}$). The sample is biased towards early-type barred galaxies, which have higher surface brightness. This morphological criteria was set to ensure that we could obtain data with enough signal-to-noise in the bar region (see Paper I). In the future, we plan to enlarge the sample towards later types to analyse the trends with morphological type. Half of our galaxies have nuclear activity to analyse possible trends between the nuclear activity, the bar characteristic of the bar and the bulge. Furthermore, eight of the galaxies present nuclear bars. Our final sample comprises 20 galaxies. For commodity, we reproduce here the Table (Table 1), already shown in Paper I, with the main characteristics of the sample as taken from the Hyperleda catalogue (Paturel et al. 2003)[1]. The bar strength shown in Table 1[2] has been taken from the literature, where strength is defined as the torque of a bar embedded in its disk (Combes & Sanders 1981), see Table 1 for the references for the individual galaxies. The nuclear types have been obtained from Verón-Cetty & Véron (2006). The sample shows a wide distribution of maximum rotational velocities (80 - 260 kms^{-1}).

As a working definition, we use a bulge size based on the kinematic and the line profile information. We consider the end of the bulge region the radius at which the σ starts decreasing after a plateau or dip. In Paper I, we noticed that it also coincides with a change in the slope of the line-strength profiles for all the indices. After analysing broad band images, as in Paper I, and also the HST images published in the literature (e.g. Comerón et al. 2010), we have also seen that this region coincides with changes in the morphology. Therefore, the bulge end defined using the kinematics is almost always coincident with the end of the nuclear structure; nuclear ring, double bar, inner spiral, etc;

---

[1] http://leda.univ-lyon1.fr

[2] Bar strength is shown here as bar–class; for assignment of bar–class to a certain bar strength, see Buta & Block 2001, it is on a scale from 0 to 6, 6 being the strongest bar

found in the broad-band images. Table 2 shows the approximate bulge and bar sizes, the latter given by the minimum ellipticity in the bar region (see Paper I for a further explanation). In Table 2 we give the central structure and bar semi-major axis size values only for those galaxies for which we have good broad-band imaging, see Paper I for a more detailed explanation. In the same paper, we present the line-of-sight position diagrams and velocity dispersion for the galaxies (figure 8). From a close examination of the stellar kinematics in the bulge region we showed that all the galaxies in the sample have disk-like structures in their centres.

Due to the presence of these disk-like structures in our galaxies, we have used, in this work, a maximum velocity dispersion instead of a central velocity dispersion. This velocity dispersion is defined as the maximum velocity dispersion in the bulge region. We have chosen this dispersion value to avoid being dominated in some galaxies by the low central velocity dispersion that could be indicative of nuclear star formation (e.g nuclear disk). Therefore, the maximum velocity dispersion should be closer to the velocity dispersion of the bulge.

3. Observations and reduction

We obtained long-slit spectra along the bar major-axis for our sample of 20 barred galaxies. The bar position angles were derived using the Digital Sky Survey (DSS) images. The observations were performed in two different runs, with the Double Beam Spectrograph at Siding Spring Observatory (Australia) and with the IDS spectrograph at the Isaac Newton Telescope (La Palma, Spain), respectively. The observations were described in detail in Paper I. To summarise, in the first run, spectra for 6 galaxies were obtained, covering a wavelength range from 3892-5815Å and a spectral resolution of FHWM~2.2Å. In the second run, spectra for 14 galaxies were obtained, covering a wavelength range of 3020-6665Å and a spectral resolution of ~3Å (FWHM).

The reduction of the two runs was carried out with the package REDUCEME (Cardiel 1999). Standard data reduction procedures (flat-fielding, cosmic ray removal, wavelength calibration, sky subtraction and fluxing) were performed. Error images were created at the beginning of the reduction and were processed in parallel with the science images. For details about the reduction steps see Paper I.

In order to derive the index spatial distribution for the fully reduced galaxy frames, a final frame was created by extracting spectra along the slit, binning in the spatial direction to guarantee a minimum signal-to-noise ratio of 20 per Å in the spectral region of Mgb. This minimum S/N ensures errors lower than 15% in most of the Lick/IDS indices (Cardiel et al. 1998). A careful emission-line removal was performed with GANDALF (Sarzi et al. 2006). The details of the procedure can be found in Paper I. This emission-line removal procedure fits simultaneously, the stellar and the emission line spectra, by treating the emission lines as additional Gaussian templates and iteratively searching for the best radial velocity and velocity dispersion. When the nebular emission-line profiles are clearly asymmetric (i.e in the nuclei of active galaxies) and cannot be fitted by a single Gaussian, double Gaussians are use to fit the emission lines.

4. Line-strength indices

Lick/IDS line-strength indices using the definition in Trager et al. (1998) were measured in all the binned spectra, cleaned of

Table 2. Bar and bulge sizes

Object	Bar semi-major axis (arcsec)	Bulge radius (arcsec)
NGC1169	29	5
NGC1358	–	5
NGC1433	–	5
NGC1530	69	15
NGC1832	–	7
NGC2217	–	5
NGC2523	–	10
NGC2665	–	5
NGC2681	23	8
NGC2273	21	5
NGC2859	48	7
NGC2935	–	7
NGC2950	44	10
NGC2962	45	5
NGC3081	35	5
NGC4245	59	6
NGC4314	92	8
NGC4394	56	5
NGC4643	67	10
NGC5101	–	7

emission, along the radius. The errors were calculated from the uncertainties caused by photon noise, wavelength calibration and flux calibration.

Line-strength indices depend on the broadening of the lines caused by instrumental resolution and by the internal motion of the stars. Before measuring the indices, we broadened our spectra to the Lick/IDS wavelength dependent resolution following the prescriptions of Worthey & Ottaviani (1997). Afterwards, we applied a correction due to the velocity dispersion of the galaxies using, for each spectrum, the template obtained in the derivation of the velocity dispersion, as described in Paper I. Offsets to transform into the Lick/IDS spectrophotometric system using stars in common with this library were derived (see Paper I). However, we only apply the offset to the indices when comparing with the Thomas et al. (2003) models based on the Lick/IDS fitting functions. To study the central and global properties of the bulges, we have also extracted the spectra in 3 different apertures by averaging line-strength indices inside 1.2, 3.6 and 10 arcsec and a fourth one averaging the indices inside the whole bulge, using the sizes given in Table 2. The process is different from adding the spectra inside those apertures and measure the indices afterwards. We decided to proceed in this way, first, to be able to compare with other authors when only line-strength indices were available but not the whole image and, secondly, to magnify the differences in the external parts of the bulges, which normally do not have much weight when a normal extraction, necessarily weighted with the light, is performed. The error is calculated as the standard error of the mean which is the standard deviation of the sampling distribution of the mean.

5. Results

In order to analyse the influence of bars in building bulges, in this section we compare the line-strength indices in the bulge of barred and unbarred galaxies. We also analyse the spatial distribution of the indices, as differences may be expected due to the differences in the gas dissipation processes and star formation events in bulges built via mergers and via secular evolution. We also compare our line-strength indices to stellar population

Table 1. General properties of the sample

Object	v(km s^{-1})	Type	Bar-class[1]	Nuclear type	Inner morph.[2]	B	V$_{max,gas}$ (km s^{-1})[3]	i(deg)
NGC 1169[a]	2387	SABb	3	–	–	12.35	259.1 ± 7.3	57.1
NGC 1358	4028	SAB(R)0	–	Sy2	–	13.19	136.1 ± 10.6	62.8
NGC 1433[b]	1075	(R)SB(rs)ab	4	Sy2	Double–bar[a]	10.81	85.1 ± 2.4	68.1
NGC 1530[b]	2461	SBb	6	–	–	12.50	169.1±3.5	58.3
NGC 1832[d]	1939	SB(r)bc	2	–	–	12.50	129.9±2.0	71.8
NGC 2217	1619	(R)SB(rs)0/a	–	LINER?	Double–bar[b]	11.36	183.4± 9.2	30.7
NGC 2273[c]	1840	SB(r)a	2	Sy2	–	12.62	192.2±5.5	57.3
NGC 2523	3471	SBbc	–	–	–	12.64	211.4 ±10.9	61.3
NGC 2665	1734	(R)SB(r)a	–	–	–	12.47	130.9±7.1	32.8
NGC 2681[c]	692	(R)SAB(rs)0/a	1	Sy3	Triple–bar[c]	11.15	87.5±6.7	15.9
NGC 2859[c]	1687	(R)SB(r)0 ^	1	Sy	Double–bar[d]	11.86	238.5±13.3	33.0
NGC 2935	2271	(R)SAB(s)b	–	–	–	12.26	188.3±2.0	42.7
NGC 2950	1337	(R)SB(r)0^ 0	–	–	Double–bar[e]	11.93	–	62.0
NGC 2962	1966	(R)SAB(rs)0	–	–	Double–bar[c]	12.91	202.9±9.9	72.7
NGC 3081[c]	2391	(R)SAB(r)0/a	3	Sy2	Double–bar[d]	12.89	99.9±4.0	60.1
NGC 4245[c]	815	SB(r)0/a	2		–	12.33	113.5±5.4	56.1
NGC 4314[a]	963	SB(rs)a	3	LINER	Double–bar[c]	11.42	253.3±24.6	16.2
NGC 4394[d]	922	(R)SB(r)b	3	LINER	–	11.59	212.5±16.0	20.0
NGC 4643[c]	1335	SB(rs)0/a	3	LINER	–	11.68	171.4±7.2	42.9
NGC 5101[d]	1868	(R)SB(r)0/a	2	–	–	11.59	195.7±9.0	23.2

(1) : (*a*) Bar class derived from the $K - band$ light distribution, Block et al. (2001)
(*b*) Bar class derived from the $K - band$ light distribution, Block et al. (2004)
(*c*) Bar class derived from the $K - band$ light distribution, Buta et al. (2006)
(*d*) Bar class derived from the $H - band$ light distribution, Laurikainen et al. (2004)
(2) : (*a*) Buta (1986) (*b*) Jungwiert et al. (1997) (*c*) Erwin (2004) (*d*) Wozniak et al. (1995)
(3) Rotational velocity corrected for inclination

models to derive SSP-equivalent ages and metallicities both, in central apertures and along the radius.

5.1. Comparison of the central line-strengths of bulges of barred and unbarred galaxies

We have mainly compared throughout the paper our results with those obtained by Moorthy et al. (2006) since the galaxy morphologies are similar in both samples. We selected those galaxies, with b/a between 0.70 and 1.00, and early type galaxies with inclinations from the literature between 10° and 70°, for which no b/a was given in Morthy et al. (2006). NGC 2787 and NGC 3945 inclinations from Erwin and Sparke (2003) and the inclination of NGC 3384 from Busarello et al. (1996). This selection matches our inclination criteria. Their low-inclination sample contains 19 galaxies, eleven of which are barred. Using these data we can also test, not only the consistency of the results, but also we can search for differences between the barred and the un–barred sample. B. Moorthy kindly provided us all the index values along the radius for their sample. This made possible to extract the indices measured in exactly the same way; same resolution (they broadened their spectra to the Lick/IDS resolution as ourselves), and same apertures as in our own data. We subtract the offsets they applied to transform their indices to Lick/IDS system. Because their study, as ours, measured the indices in flux-calibrated spectra at the Lick/IDS resolution, there should not be additional offsets between their and our line-strengths values.

Figure 1 shows the variation of three representative indices inside an aperture of 1.2, 3.6 and 10.0 arcsec vs. σ. As it can be seen all bulges with $\sigma > 150$ km s^{-1} have almost the same index values (except for Mgb and CN$_2$, not shown in the figure), while there is a large scatter in the index-values for bulges with with $\sigma < 150$ km s^{-1} This behaviour has already been noticed

by several authors in elliptical galaxies (see, e.g, Caldwell, Rose & Concannon 2003; Nelan et al. 2005; Sánchez-Blázquez et al. 2006; Ogando et al. 2006). There is a tendency in the metallicity sensitive indices for the barred galaxies to be larger than those derived for unbarred galaxies while the opposite is observed for the Balmer indices. We have performed a significance test (3 σ) on the index distributions with σ. For some of the indices, namely, the Balmer indices, Fe4383 and Mgb there is a statistically significant difference between the bulges of barred and unbarred galaxies at all apertures while for the other indices the difference is not statistically significant.

In Sec 6 we compare the line-strength with stellar population models to transform the differences in differences in stellar population parameters (name it, age, metallicity ([Z/H]) and relative abundance of α-elements ([E/Fe]).

We have not seen that the AGN presence affects the calculated line-strength values after comparing the values for galaxies with and without an AGN nucleus.

5.2. Comparison of the central line-strengths of bulges and elliptical galaxies

Due to the proposed continuation of properties between bulges and elliptical galaxies (e.g. Kuntschner et al. 2006), we would like to compare our results with those obtained for elliptical galaxies. Figure. 2 shows the central Mgb, Hβ, Fe5015 and Mgb/F5015 values against the σ, together with the values presented in Kuntschner et al. (2006) for a sample of ellipticals and S0's. For reference, we have also plotted the values for the late-type galaxies in Ganda et al. (2007), which covers the same indices and spectral resolution as Kuntschner et al. (2006) data. We have also plotted the sample by Moorthy et al. (2006) studied here. There is a tight correlation between σ and Mgb. The trend of Hβ, Fe5015 indices with σ for all the galaxies is almost
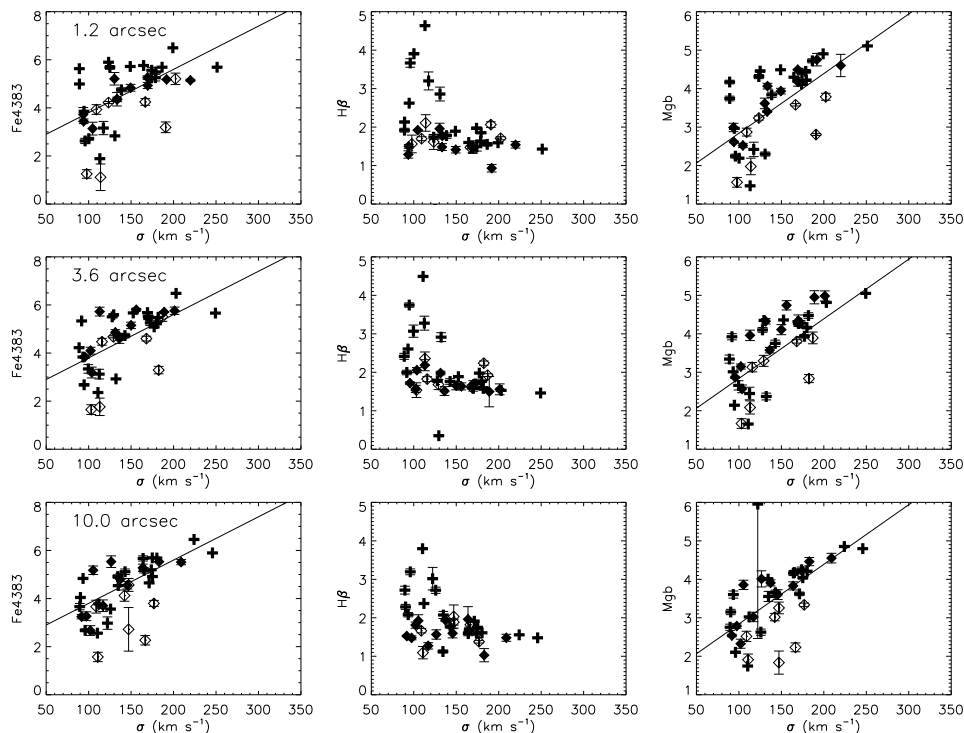
Fig. 1. Distribution of three representative central averaged indices vs. σ for our galaxies and Moorthy et al galaxies; 1.2 arcsec average (top panel), averaged 3.6 arcsec (middle panel) and averaged 10.0 arcsec (bottom panel). Empty symbols represent unbarred galaxies, while filled symbols represent barred galaxies with the crosses being our galaxies and the diamonds Moorthy's sample.

flat, showing a large dispersion for galaxies with maximum velocity dispersion below 150km s^{-1}. The spread is also larger for the galaxies classified as barred. The central Fe5015 index of the unbarred galaxies seems to follow more closely the values of ellipticals while the Mgb follows the opposite trend, with barred galaxies showing values more similar to those of elliptical galaxies. This results in a Mgb / Fe5015 ratio where the central values of unbarred galaxies follow more closely those of ellipticals while the barred galaxies tend to lie above those values for the larger central velocity dispersion galaxies. Those galaxies showing the lower Mgb values are also the ones with lower Balmer indices.

It is interesting to notice that although Thomas & Davies (2006) found that, at fixed σ, ellipticals and the bulges of early–type galaxies are indistinguishable, their sample did not contain any barred galaxies. However, Moorthy et al. (2006) found that for a given σ the bulges of barred and unbarred galaxies show differences similar to those found by us with a larger sample. The implications of these results will be discussed in Section 7.

5.3. Line-strength distribution gradients

The variation of the indices with radius in the bulge region was presented in Paper I. The distribution of the indices in the bulge regions is, in some of the cases, far from a linear one. The distribution of the Balmer index is generally characterised by a maximum in the bulge region, close to the bulge end. These profiles are due to the presence of central structures such as nuclear rings. Despite this non–linear distribution and in order to quantitatively characterise the gradients, we have performed a linear fit to the data in the bulge region. Tables in Appendix A.1 show the gradients resulting from the fit to the indices for each of the galaxies.

Most galaxies show negative or no gradients in their metallicity sensitive indices and positive or null gradients in their Balmer indices. NGC 2273 and NGC 2665 show a small positive gradient in their metallicity sensitive indices. NGC 1832 and NGC 2217 also show this trend in their metallicity sensitive indices but it is likely due to the presence of an nuclear ring in the outer part of the bulge. In the case of a long–lasting ring we would expect an enrichment of the ring area due to a continuous star formation activity.

Previous studies of line–strength gradients in bulges (Moorthy et al. 2006; Jablonka et al. 2007; Morelli et al. 2008) also find that most galaxies show negative gradients in the metallicity sensitive indices. With respect to the age sensitive gradients (i.e. Balmer indices), Moorthy et al. find that in the cases that a positive age gradient is present it is always in a barred galaxy. In our case, where only barred galaxies are analised, we find galaxies with a variety of index distribution with negative, positive or null Balmer indices gradients. The galaxies which show a negative gradient seems to be associated to the presence of a nuclear ring.

6. Ages and metallicities

In order to transform our measured indices into single stellar population equivalent parameters, we use two different set of models. The first one, from Vazdekis et al. (2010)[3], is built using the MILES library (Cenarro et al. 2007; Sánchez-Blázquez et al. 2006). The second set of models we use is that of Thomas, Maraston & Bender (2003) which are based on the Lick/IDS fitting functions (Gorgas et al. 1993; Worthey 1994). These two set of models use different isochrones and stellar libraries and

---

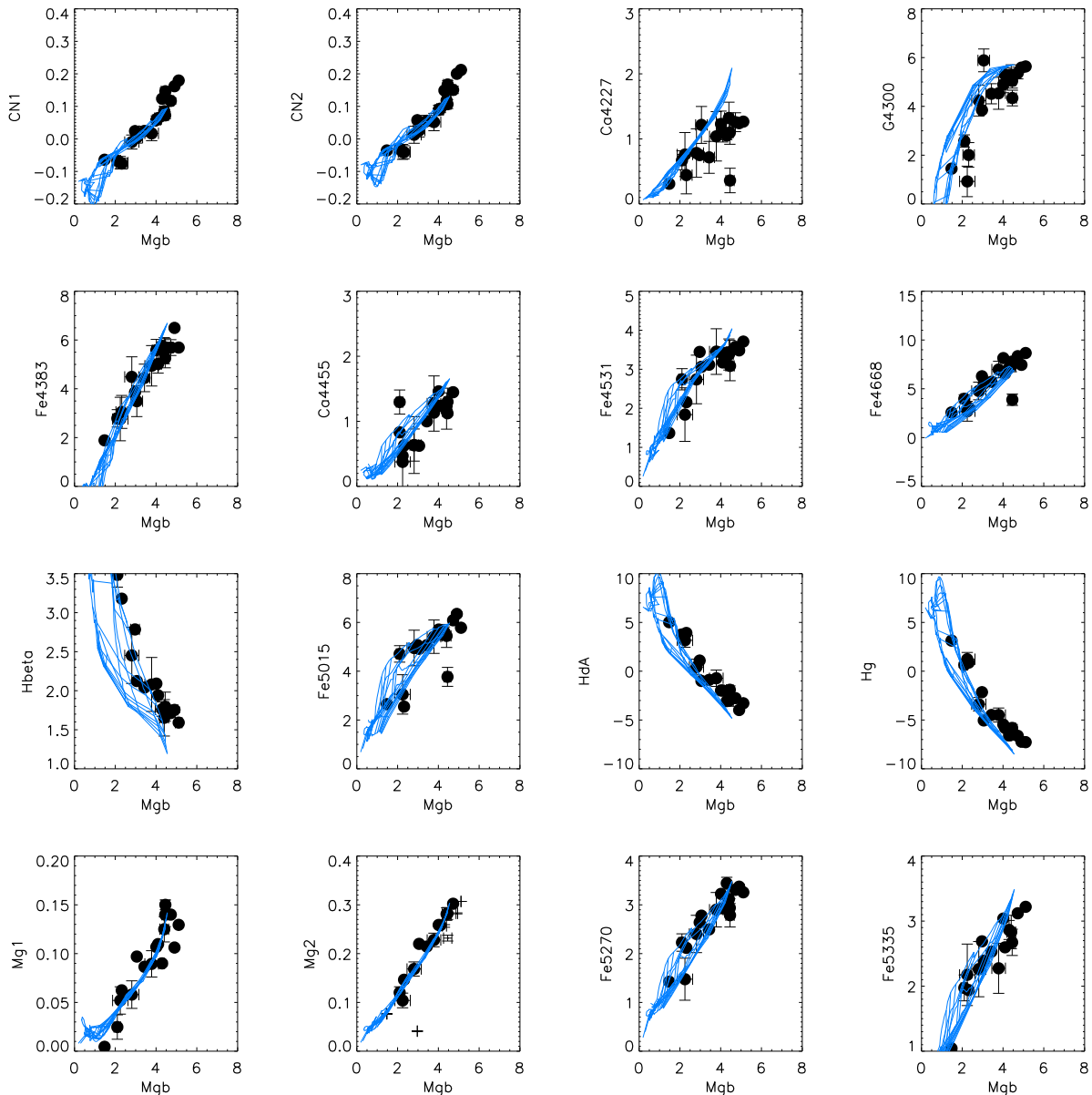[3] The models are publicly available at http://miles.iac.es

Fig. 3. Central index vs. central Mgb From top to bottom and from left to right; CN1, CN2, Ca4227, G4300, Fe4383, Ca4455, Fe4531, C4668, Hβ, Fe5015, H$_\delta$, H$_\gamma$, Mg1, Mg2, Fe5270, Fe5335. Over-plotted are the models by Vazdekis et al. (2010) for a range of ages (0.5 to 18 Gyr) and metallicities (-1.68 to 0.0)

the comparison between the results obtained with them can be used as an estimation of the errors affecting the predictions. The details about the uncertainties are carefully discussed in Paper I. It is clear that the true star formation history in these objects will be more complicated than a simple SSP. However, very useful information can still be retrieved from the SSP analysis if they are properly interpreted. Roughly, the SSP-equivalent age of a composite stellar population (CSP) is dominated primarily by the age of the youngest component and the mass fraction of the different populations. The SSP-equivalent metallicity is very similar to a $V - band$ luminosity weighted chemical composition (Serra &Trager 2007). Fig. 3 shows the central line indices vs. the central Mgb, with the Vazdekis et al. (2010) models overplotted. The plot shows a tight correlation among the different indices for the central region and very good agreement with

the models except for some well-known exceptions. In particular, some galaxies show values of CN, Mgb, G4300 and C4668 that are larger than the models while this is not true for the Fe-sensitive indices. This can be reflecting and overabundance of Mg/Fe and probably C/Fe and N/Fe with respect to the solar neighbourhood, as suggested by many authors (e.g. Worthey 1998; Tantalo et al 1998; Trager et al. 2000; Sánchez-Blázquez et al. 2003; Graves & Schiavon 2008). Similarly to Paper I, to obtain stellar population parameters we use 4 indices, namely; HδA, HγA, Fe4383 and Mgb and follow a multi-index approach as described in Proctor & Samson (2002), a detailed explanation of the error calculation is given in Paper I.

The SSP-equivalent age and metallicity distributions along the radius are shown in Fig. 4. As well as for our data, we have also derived the ages and metallicities in the way explained in
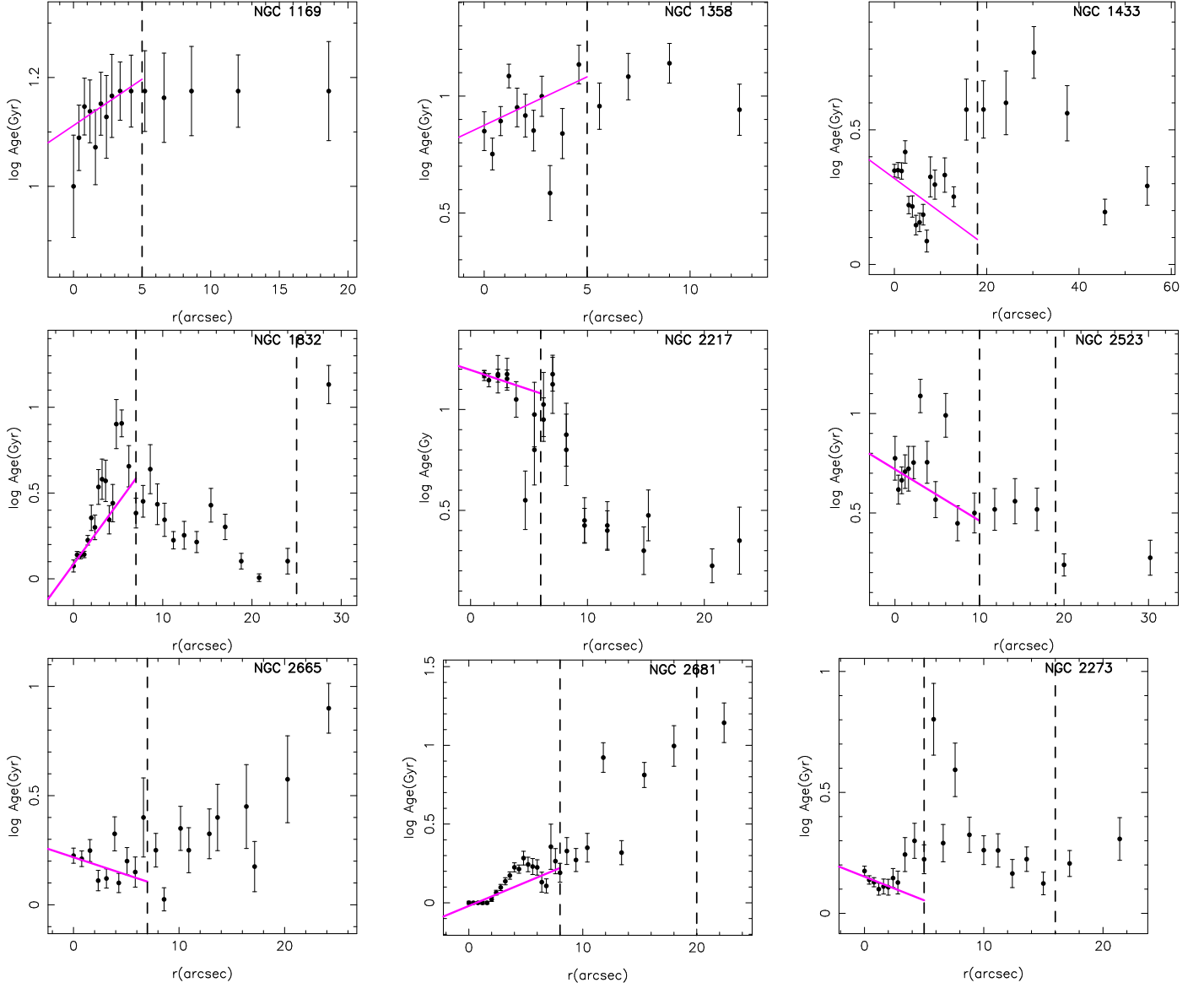
Fig. 4. SSP-equivalent age and metallicity along the radius. Dashed lines indicate the end of the bulge and the bar region respectively. A linear fit to the bulge region is also plotted.

Paper I for the data published by Moorthy et al. (2006). From Fig. 5 it can be seen that the metallicity and ages in both barred and unbarred galaxies seem to cover the same range of values, but barred galaxies tend to have higher metallicities than unbarred galaxies at a given σ. No clear difference is found for the central ages. The [E/Fe] values for unbarred galaxies tend to lie below the values of barred galaxies at a given σ. When we open the aperture, to include the whole bulge, the trends become clearer, with the metallicities of the unbarred galaxies lying below those of the barred galaxies at a given σ. Also the [E/Fe] is still remains lower for the unbarred galaxies when the aperture is as large as the whole bulge region. Similar results are found when comparing with elliptical galaxies (see Fig. 2 and Sect. 5.1) although in that case, we have just compared the Mgb / Fe5015 ratio. However, these trends are week, and a significance test applied on the stellar parameters does not reveal any statistically significant difference. Although the low number of unbarred galaxies might be driving the significance test. At this point, due to the large dispersion of the values, and the lack

of statistical significance, this apparent trend on the [E/Fe] values should be confirmed in the future with a larger set of data. The results on the bulge metallicity confirm the bulge spectral indices trends (see Sect. 5.1) where we found that the metallicity sensitive indices of barred galaxies are larger than those of unbarred galaxies.

6.1. Age and metallicity gradients

Linear fits have been performed on the derived ages, metallicities and [E/Fe] values vs. radius (see Table 3). Figure 4 shows the radial distribution of ages and metallicities for all the galaxies. Fig. 6 shows that, on average, galaxies with lower σ tend to have negative age gradients while larger central velocity dispersion galaxies show positive age gradients. The relation between [Z/H] gradient and the central velocity dispersion is shown in Fig. 6. Most galaxies show a negative [Z/H] gradient. The mean metallicity gradient is -0.19 ± 0.07 dex for the barred galaxies and -0.3± 0.1 for the non-barred ones (notice that these gradi-
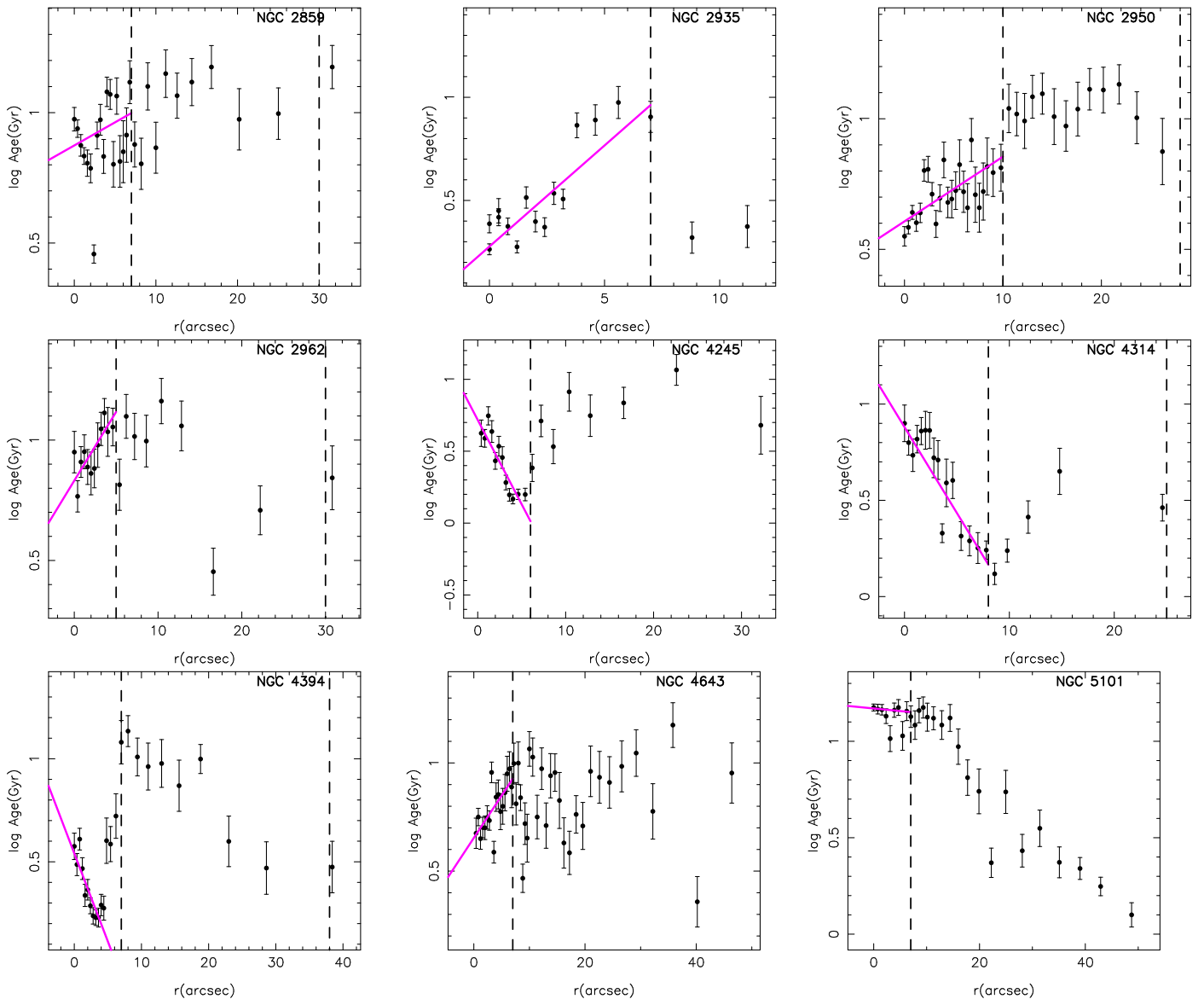
Fig. 4. continued.

ents are calculated using log scale for the radius to be able to compare with the literature, while the gradients given in Table 3 and Fig. 6 have been derived using a linear scale). Both values are within the values obtained by other authors for the bulge of galaxies. For example, Morelli et al. found a mean value of (-0.15 dex) and Jablonka et al. (2007), d[Z/H]/dr=-0.2 dex for a sample containing both, barred and non-barred galaxies.

The differences between the metallicity gradient of barred and non-barred galaxies are not statistically significant. We also do not find a correlation between the metallicity gradient of barred galaxies and the central velocity dispersion. In early-type galaxies, a possible correlation between the metallicity gradient and the mass for elliptical galaxies with central sigma ≤150-175 km/s has been claimed (Sánchez-Blázquez et al. 2007; Spolaor et al. 2009; Kuntschner et al. 2010). Other studies, for both, early-type galaxies (Ogando et al. 2005) and bulges (Jablonka et al. 2007) found a lower boundary instead of a correlation in the sense that massive galaxies do not show strong gradients but less massive galaxies show a larger scatter. In our sample we do not observe neither a correlation or a lower boundary and, after comparison with the data from Jablonka et al. 2007, our gra-

dients are distributed similarly to their gradients and therefore, there is no systematic effect affecting our results. Very high S/N data might help to answer whether there is a real correlation between metallicity gradients and velocity dispersion. [E/Fe] gradients are shown in Fig 6. The [E/Fe] gradients are very small, almost compatible with being null, although they take both positive and negative values. Bulges with low velocity dispersion (σ < 100km s^{-1}) tend to have systematically positive values, while the same is not true for more massive bulges. In any case, the values of the gradients are, as said above, very small. This is compatible with what is found in elliptical galaxies, where also the [E/Fe] is found to be compatible with zero in most cases (e.g., Mehlert et al. 2003; Sanchez-Blazquez et al. 2006, 2007) and in other studies of bulges (e.g., Jablonka et al. 2007; MacArthur et al. 2009). For comparison, we have also derived, in a similar way, age, metallicity and [E/Fe] gradients for Moorthy's sample. The values of the barred galaxies in this sample coincide with those of our galaxies and we do not find difference between the values of barred and unbarred galaxies. The interpretation of the gradients is complicated as their value may change due to many different physical processes and also because substruc-
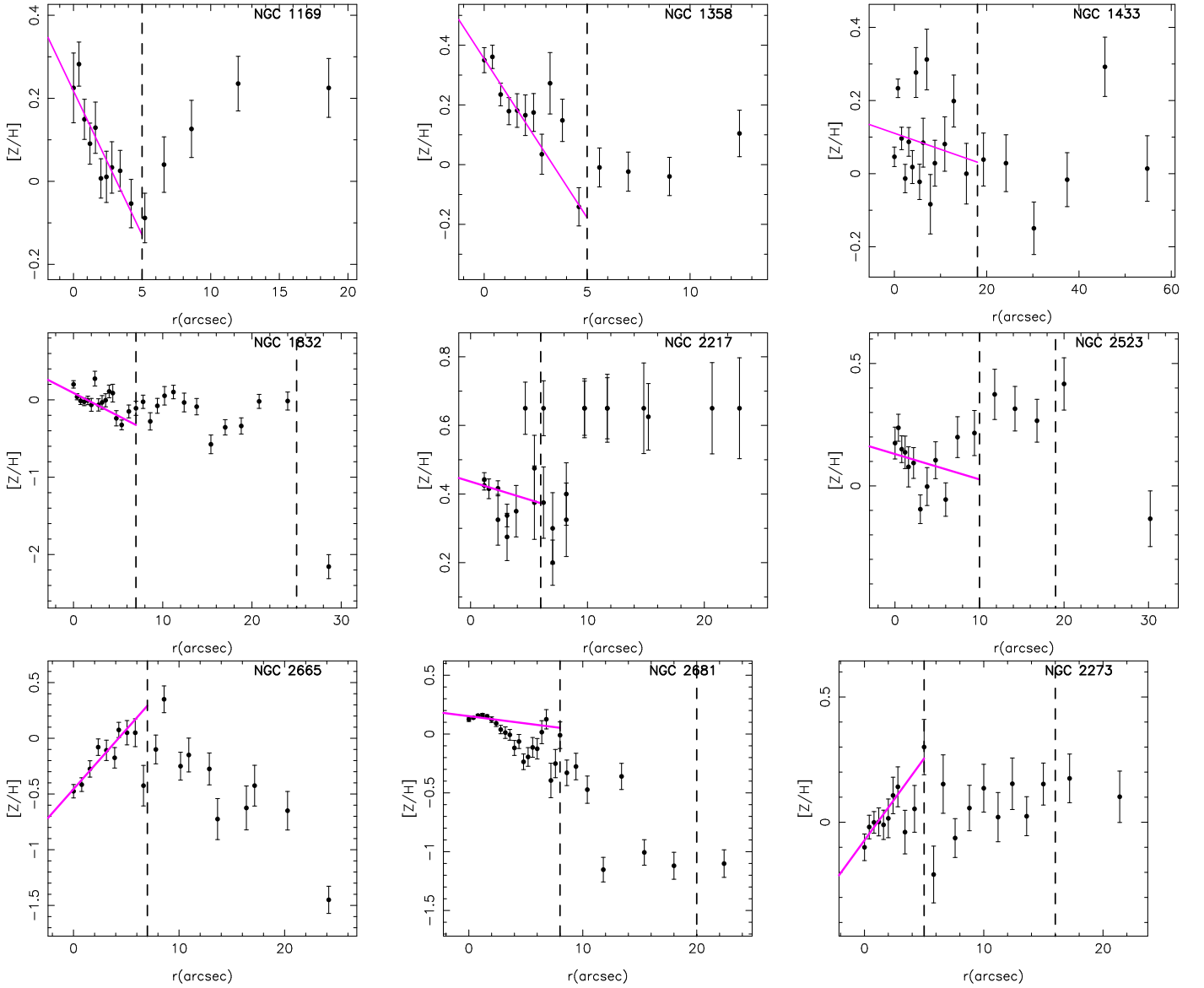
Fig. 4. continued.

tures inside the galaxy, as rings, disks, etc, which are common in our sample, change the value of the slope which is intrinsic to the spheroid.

6.2. Comparison between the SSP stellar parameters in the bulge and the bar region

It is interesting to relate the bulge mean age and metallicity gradients to the gradients and mean values in the bar region because in Paper I, we found seven galaxies with metallicity gradients in the bar region significantly (more than 3-σ significance) different from zero: NGC 1169, NGC 2217, NGC 4394, and NGC 5101 (positive) NGC 2665, NGC 2681, NGC 4245 (negative), we excluded from this analysis NGC 1530, NGC 3081, NGC 4314 and NGC 2935 due to the large fitting errors in the bar region. In Fig. 7 we can see the relation between the mean metallicities in the bulge and the bar region. It is striking the good correlation between the metallicities in both the bar and the bulge. This results points to a bulge enrichment linked to that of the bar.

Although the mean values of both bars and bulges are correlated, the bulge gradients do not show any correlation with the bar gradients, being the bulge gradients more indicative of the presence of morphological substructures in the bulge.

7. Summary and discussion

Following the results from Pérez et al. (2009) for the stellar line-strength indices and the ages and metallicities distribution along the bars of a sample of 20 galaxies, we have carried out a detailed study of the populations of the central regions of those galaxies. We have compared the results with the bulge properties of a similar sample of unbarred galaxies (Moorthy et al. 2006), deriving the SSP equivalent stellar parameters in the same way as for our sample. We have found differences in the bulge stellar population properties between barred and unbarred galaxies. We find that some of the metallicity sensitive indices of the bulges of barred galaxies lie above those of unbarred galaxies and the Balmer indices tend to follow the opposite trend, as was already hinted by Moorthy et al. (2006). It is interesting to note that although one could say that there is a good correlation between
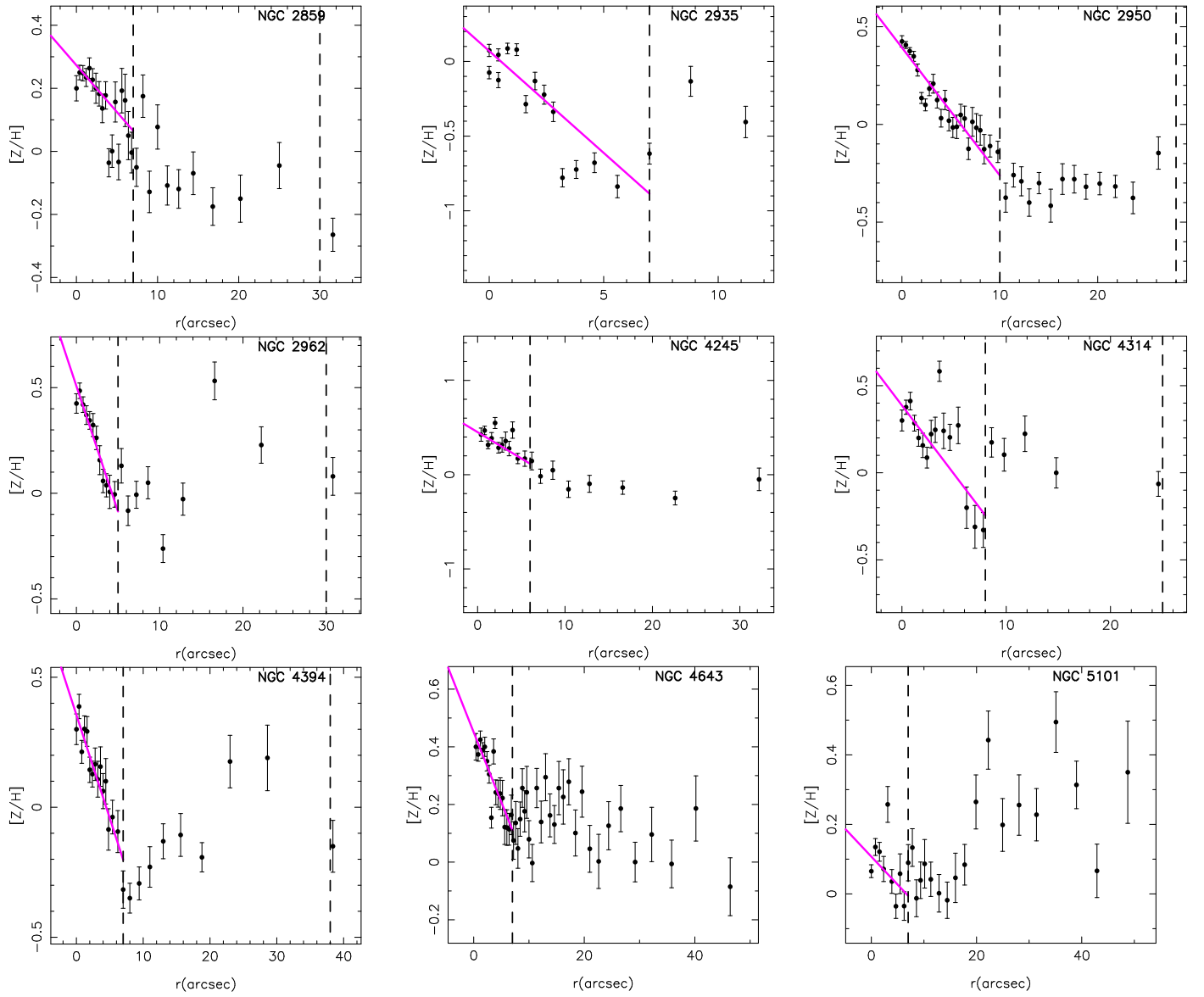
Fig. 4. continued.

Table 3. Linear fit age and metallicity gradients to the bulge region

Name	Age grad	err	[Fe/H] grad	err	[E/Fe]	err	[Z/H]	err
N1169	0.017	0.005	−0.064	0.013	−0.007	0.008	−0.069	0.015
N1358	0.041	0.034	−0.105	0.013	0.002	0.004	−0.106	0.013
N1433	−0.013	0.007	−0.001	0.009	0.010	0.005	−0.004	0.011
N1832	0.071	0.025	−0.061	0.020	0.017	0.008	−0.059	0.014
N2217	−0.019	0.017	−0.030	0.019	−0.024	0.008	−0.010	0.033
N2523	−0.026	0.009	0.010	0.006	−0.005	0.003	−0.010	0.013
N2665	−0.016	0.013	0.121	0.028	−0.020	0.010	0.107	0.017
N2681	0.030	0.011	−0.021	0.014	0.001	0.006	−0.012	0.018
N2273	−0.019	0.012	0.070	0.018	−0.010	0.010	0.065	0.015
N2859	0.018	0.015	−0.037	0.006	−0.037	0.006	−0.030	0.006
N2935	0.098	0.022	−0.121	0.021	−0.022	0.010	−0.136	0.025
N2950	0.025	0.009	−0.069	0.004	−0.004	0.004	−0.065	0.008
N2962	0.057	0.015	−0.105	0.009	0.001	0.006	−0.119	0.011
N4245	−0.117	0.023	−0.025	0.022	0.004	0.008	−0.056	0.013
N4314	−0.089	0.015	−0.057	0.020	0.010	0.008	−0.079	0.017
N4394	−0.085	0.017	−0.087	0.011	0.023	0.006	−0.079	0.009
N4643	0.039	0.007	−0.043	0.006	−0.003	0.002	−0.048	0.006
N5101	−0.007	0.005	−0.026	0.013	0.007	0.005	−0.016	0.014

Fig. 5. Age, [Z/H] and [E/Fe] for the average central 10 and 3.6 arcsec apertures. Symbols as in Fig. 1

line-strength indices and σ, it would be a better description of the index distribution with σ to say that there is a almost constant value of the indices with σ plus a tail in the distribution for the smaller σ galaxies (below $\approx$150km s^{-1}). Most galaxies show negative gradi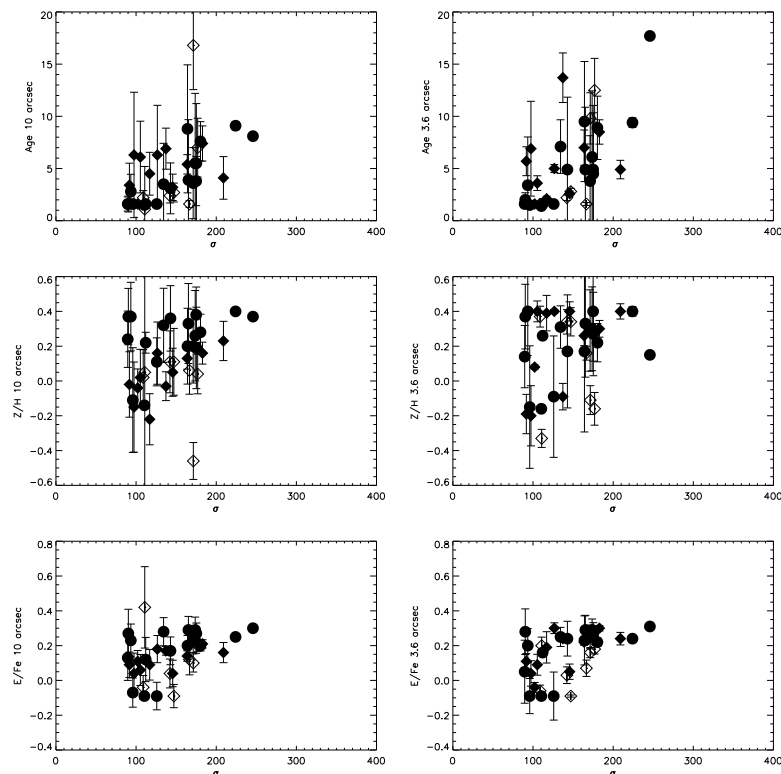ents for metal-sensitive indices while the opposite is true for Balmer line indices, although NGC 1832 and NGC 2665 show clearly the opposite trend. The index distributions are closely linked to morphological substructures in the bulge region such as nuclear rings.

We have derived the ages, metallicities and [E/Fe] values using two different set of models. The central parts of barred galaxies tend to be more metal rich than the unbarred counterparts. Interestingly, [E/Fe] seems to be enhanced for the barred galaxies over the unbarred central regions. Although, due perhaps to the low number of unbarred galaxies in the sample, these trends are not statistically significant and would need to be followed up with a larger sample of unbarred galaxies. The age gradients follow the index trend with σ, most galaxies show no gradient or slightly positive gradient; however, the distribution of gradients for galaxies with σ below $\approx$ 150km s^{-1} shows a larger dispersion. The same behaviour is found for the metallicity trends, with most values being negative, with grad[Fe/H] around -0.05, the only outliers are found in galaxies with σ below 150km s^{-1}. Galaxies with σ above 150km s^{-1} show a null [E/Fe] gradient while galaxies with central velocity dispersion below this value show a positive [E/Fe] gradient. We have calculated the gradients also in Moorthy's data. There is a very good agreement in the values of both samples and we do not find any difference between barred and unbarred galaxies. The interpretation of the gradients is difficult as there are too many processes that can modify their shape. Furthermore, the presence of substructures,

as disks or rings, which are very common in our sample, makes very difficult to measure the real gradient of the spheroid.

The fact that barred galaxies show a similar age and a lower [E/Fe] is, in principle, a puzzling result. In a classical scenario of secular building of the bulge, the star formation extends for much longer timescales than in a merger built scenario, where star formation happens very efficiently and in short period of times. On the contrary, we are finding (in agreement with Moorthy et al. 2006), completely the opposite result. One possible bias to this study is that our sample contains, mostly, early-type spirals. We showed, in Paper I, that the bars in these galaxies are old and have high values of E/Fe (see also Gadotti & de Souza 2006). The epoch of formation of these bars is probably associated with the epoch of formation of the bulge, which would be compatible with the strong correlation we find in the stellar parameters of both components. Some proposed mechanisms to form bars are, e.g., mergers and interactions. These processes can create both, the bar and the bulge, in particular in those galaxies with early type morphologies (see, e.g., Walker et al. 1996; Berentzen et al. 2004; Peirani et al. 2009). In this scenario, it could well happen that this mechanism created both, the bar and the bulge, in some galaxies, in particular those with early-type morphologies. During the formation of the bulge, the star formation could have been enhanced by the presence of this bar, increasing the metallicity and the [E/Fe] values of the bulge with respect to those bulges lacking this structure (e.g. Pérez & Freeman 2006). Later accretion of gas can then be funneled towards the center forming nuclear discs and rings (Emsellem et al. 2001; Wozniak et al. 2003, Wozniak & Champavert 2006), producing substructures with low level of star formation, i.e. slightly younger (showing a lower SSP-equivalent age in our data), but that would not contain enough
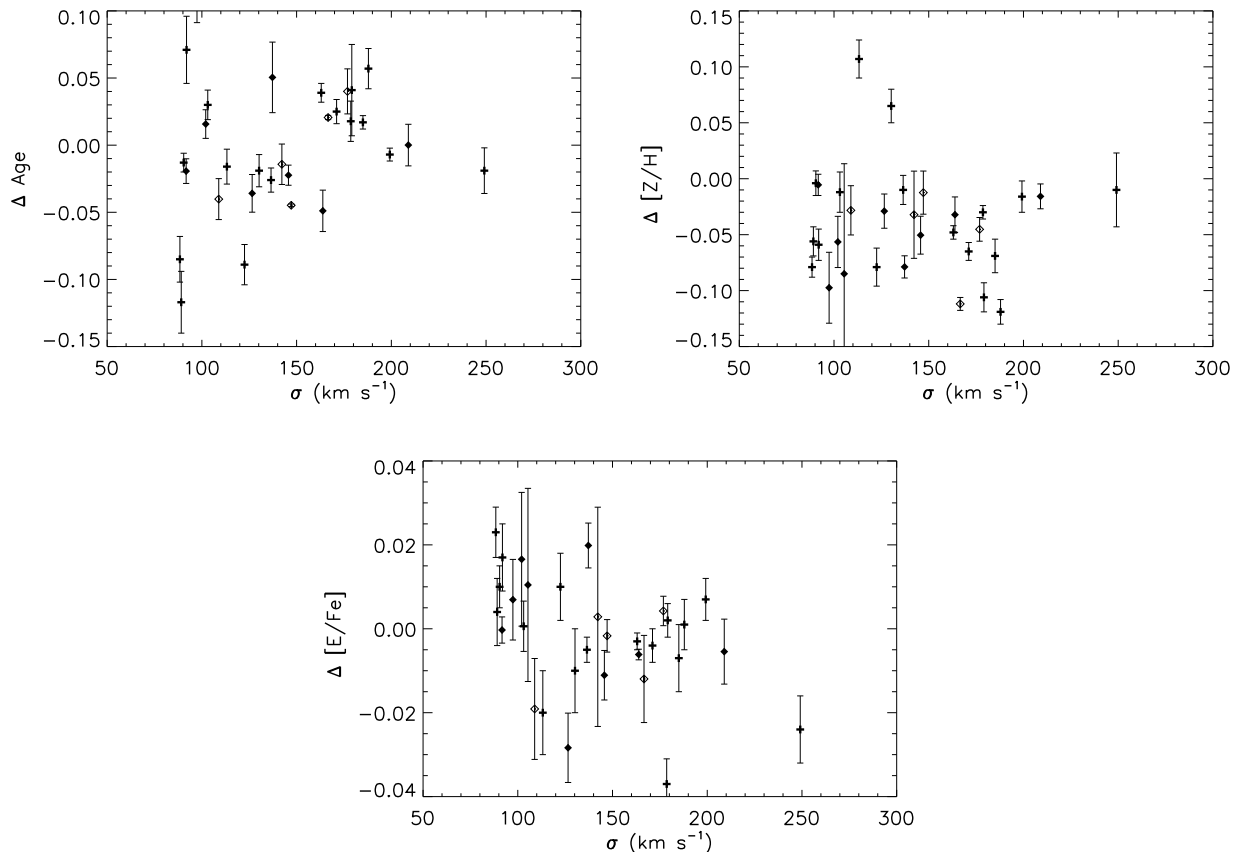
Fig. 6. Age, [Z/H] and [E/Fe] gradient in the bulge region vs. maximum central dispersion. Symbols as previous figures, i.e empty symbols representing unbarred galaxies, while filled symbols represent barred galaxies with the crosses being our galaxies and the diamonds represent Moorthy's galaxies for which a reliable gradient could be obtained.

stars to produce a change in the SSP-equivalent metallicities and [E/Fe] as the metallicity and [E/Fe] values reflect more the values of the dominant (in mass) stellar population (see Serra & Trager 2007), while the SSP-equivalent age are very bias towards the youngest components. In order to test this hypothesis, further work and analysis would be needed to derive star formation histories. If this hypothesis is confirmed, it would imply that bars are old and long lasting features and that bar formation is, at least for this early type barred galaxies, closely linked to the formation of the bulge. Due to the large dispersion in the values for some of the trends found in this study, in order to confirm them, we will need in a future work to extend the unbarred galaxy sample and the morphological range covered by it.

References

Berentzen, I., Athanassoula, E., Heller, C. H., & Fricke, K. J. 2004, MNRAS, 347, 220
Block, D., Buta, R., Knapen, J., Elmegreen, D., & Puerari, I. 2004, AJ, 128
Block, D., Puerari, I., Knapen, J., et al. 2001, A&A, 375, 761
Busarello, G., Capaccioli, M., D'Onofrio, M., et al. 1996, A&A, 314, 32
Buta, R. 1986, ApJS, 61, 609
Buta, R. & Block, D. L. 2001, ApJ, 550, 243
Buta, R., Laurikainen, E., Salo, H., Block, D., & Knapen, J. 2006, AJ, 132
Caldwell, N., Rose, J. A., & Concannon, K. D. 2003, AJ, 125, 2891
Cardiel, N. 1999, Ph.D. Thesis
Cardiel, N., Gorgas, J., Cenarro, J., & González, J. 1998, A&AS, 127, 597
Cenarro, A. J., Peletier, R. F., Sánchez-Blázquez, P., et al. 2007, MNRAS, 374, 664
Combes, F., Debbasch, F., Friedli, D., & Pfenniger, D. 1990, A&A, 233, 82
Combes, F. & Sanders, R. 1981, A&A, 96
Comerón, S., Knapen, J. H., Beckman, J. E., et al. 2010, MNRAS, 402, 2462
de Vaucouleurs, G. 1948, Ann. Astrophys., 11, 24
Emsellem, E., Greusard, D., Combes, F., et al. 2001, A&A, 368, 52
Erwin, P. 2004, A&A, 415
Erwin, P. & Sparke, L. S. 2003, ApJS, 146, 299
Falcón-Barroso, J., Peletier, R. F., & Balcells, M. 2002, MNRAS, 335, 741
Fisher, D. B. 2006, ApJ, 642, L17
Fisher, D. B. & Drory, N. 2008, AJ, 136, 773
Fisher, D. B. & Drory, N. 2010, ApJ, 716, 942
Freeman, K. C. 1970, ApJ, 160, 811
Friedli, D. & Benz, W. 1995, A&A, 301, 649
Gadotti, D. & de Souza, R. 2006, ApJS, 163
Gadotti, D. A. 2009, MNRAS, 393, 1531
Ganda, K., Peletier, R. F., McDermid, R. M., et al. 2007, MNRAS, 380, 506
Gorgas, J., Faber, S., Burstein, D., et al. 1993, ApJS, 86
Goudfrooij, P., Gorgas, J., & Jablonka, P. 1999, Ap&SS, 269, 109

Fig. 7. Average metallicity values of the bulge and the bar region (from Paper I) for the sample galaxies.
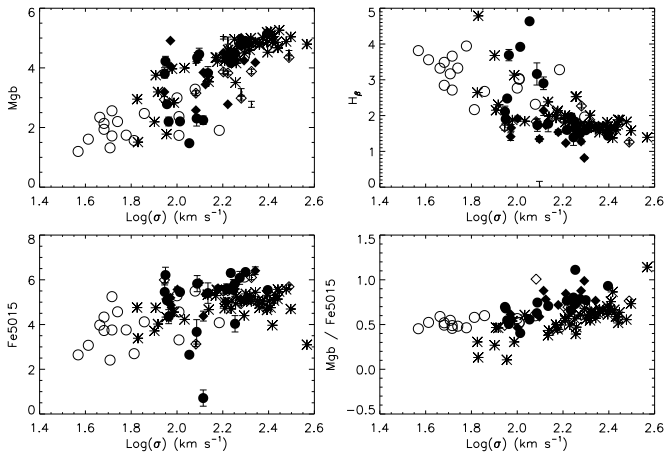
Fig. 2. Central 1.2 arcsec indices for a reference sample of late spirals, Ganda et al. (2007), open circles; a sample of ellipticals from Kuntschner et al. (2006), stars; unbarred galaxies used in this work from Moorthy et al. (2006), open diamonds; barred galaxies used in this work from Moorthy et al. (2006), filled diamonds, and the filled circles represent the values from our sample of barred galaxies.

Graves, G. J. & Schiavon, R. P. 2008, ApJS, 177, 446
Hopkins, P. F., Bundy, K., Hernquist, L., Wuyts, S., & Cox, T. J. 2010, MNRAS, 401, 1099
Jablonka, P., Gorgas, J., & Goudfrooij, P. 2007, A&A, 474, 763
Jungwiert, B., Combes, F., & Axon, D. J. 1997, A&AS, 125, 479
Kormendy, J. & Kennicutt, Jr., R. C. 2004, ARA&A, 42, 603
Kuntschner, H., Emsellem, E., Bacon, R., et al. 2006, MNRAS, 369, 497
Laurikainen, E., Salo, H., Buta, R., & Vasylyev, S. 2004, MNRAS
MacArthur, L. A., González, J. J., & Courteau, S. 2009, MNRAS, 395, 28
Mehlert, D., Thomas, D., Saglia, R. P., Bender, R., & Wegner, G. 2003, A&A, 407, 423
Moorthy, B. & Holtzman, J. 2006, MNRAS, 371, 583
Nelan, J. E., Smith, R. J., Hudson, M. J., et al. 2005, ApJ, 632, 137
Ogando, R. L. C., Maia, M. A. G., Chiappini, C., et al. 2005, ApJ, 632, L61
Ogando, R. L. C., Maia, M. A. G., Chiappini, C., et al. 2006, in Revista Mexicana de Astronomia y Astrofisica Conference Series, Vol. 26, Revista Mexicana de Astronomia y Astrofisica Conference Series, 119–120
Paturel, G., Petit, C., Prugniel, P., et al. 2003, A&A, 412, 45
Peirani, S., Hammer, F., Flores, H., Yang, Y., & Athanassoula, E. 2009, A&A, 496, 51
Peletier, R., Falcón-Barroso, J., Bacon, R., et al. 2007, MNRAS, 379
Peletier, R. F. 2008, in Astronomical Society of the Pacific Conference Series, Vol. 390, Pathways Through an Eclectic Universe, ed. J. H. Knapen, T. J. Mahoney, & A. Vazdekis, 232–+
Pérez, I. & Freeman, K. 2006, A&A, 454, 165
Pérez, I., Sánchez-Blázquez, P., & Zurita, A. 2007, A&A, 465
Pérez, I., Sánchez-Blázquez, P., & Zurita, A. 2009, A&A, 495, 775

Pfenniger, D. & Friedli, D. 1991, A&A, 252, 75
Pfenniger, D. & Norman, C. 1990, ApJ, 363, 391
Proctor, R. N. & Sansom, A. E. 2002, MNRAS, 333, 517
Sánchez-Blázquez, P., Forbes, D. A., Strader, J., Brodie, J., & Proctor, R. 2007, MNRAS, 377, 759
Sánchez-Blázquez, P., Gorgas, J., Cardiel, N., Cenarro, J., & González, J. J. 2003, ApJ, 590, L91
Sánchez-Blázquez, P., Peletier, R. F., Jiménez-Vicente, J., et al. 2006, MNRAS, 371, 703
Sarzi, M., Falcón-Barroso, J., Davies, R. L., et al. 2006, MNRAS, 366, 1151
Serra, P. & Trager, S. 2007, MNRAS, 374
Simkin, S. M., Su, H. J., & Schwarz, M. P. 1980, ApJ, 237, 404
Spolaor, M., Proctor, R. N., Forbes, D. A., & Couch, W. J. 2009, ApJ, 691, L138
Tantalo, R., Chiosi, C., & Bressan, A. 1998, A&A, 333, 419
Thomas, D. & Davies, R. L. 2006, MNRAS, 366, 510
Thomas, D., Maraston, C., & Bender, R. 2003, MNRAS, 339, 897
Trager, S. C., Faber, S. M., Worthey, G., & González, J. J. 2000, AJ, 119, 1645
Trager, S. C., Worthey, G., Faber, S. M., Burstein, D., & Gonzalez, J. J. 1998, ApJS, 116, 1
Vazdekis, A., Sánchez-Blázquez, P., Falcón-Barroso, J., et al. 2010, MNRAS, 477
Verón-Cetty, M.-P. & Véron, P. 2006, A&A, 455
Walker, I. R., Mihos, J. C., Hernquist, L., Bolte, M., & Mendes de Oliveira, C. 1996, in Astronomical Society of the Pacific Conference Series, Vol. 91, IAU Colloq. 157: Barred Galaxies, ed. R. Buta, D. A. Crocker, & B. G. Elmegreen, 486–+
Worthey, G. 1994, ApJS, 95, 107
Worthey, G. 1998, PASP, 110, 888
Worthey, G. & Ottaviani, D. L. 1997, ApJS, 111, 377
Wozniak, H. & Champavert, N. 2006, MNRAS, 369, 853
Wozniak, H., Combes, F., Emsellem, E., & Friedli, D. 2003, A&A, 409, 469
Wozniak, H., Friedli, D., Martinent, L., Martin, P., & Bratschi, P. 1995, A&A, 111

Appendix A: Linear fits to the line–strength distribution in the bulge region

Table A.1. Linear fit parameters (Y=a+bx) in the bulge region of NGC 1169

Index	a	err a	b	err b
$H\delta_A$	−3.005	0.180	0.028	0.090
$H\delta_F$	−0.088	0.124	0.0140	0.063
CN_1	0.088	0.008	−0.004	0.004
CN_2	0.120	0.009	−0.002	0.004
Ca4227	1.271	0.069	0.017	0.034
G4300	5.179	0.163	0.197	0.080
$H\gamma_A$	−6.385	0.210	−0.186	0.103
$H\gamma_F$	−2.036	0.099	0.087	0.048
Fe4383	5.480	0.163	0.059	0.078
Ca4455	1.308	0.083	−0.078	0.040
Fe4531	3.507	0.100	−0.171	0.051
C4668	7.685	0.302	−0.508	0.146
$H\beta$	1.621	0.112	0.065	0.054
Fe5015	5.671	0.151	−0.247	0.073
Mg_1	0.128	0.003	−0.004	0.001
Mg_2	0.287	0.003	−0.009	0.001
Mgb	4.484	0.073	−0.133	0.036
Fe5270	3.221	0.108	−0.161	0.053
Fe5335	3.065	0.083	−0.217	0.040

Table A.2. Linear fit parameters (Y=a+bx) in the bulge region of NGC 1358

Index	a	err a	b	err b
HdA	-1.890	0.188	0.029	0.093
HdF	0.246	0.100	0.142	0.049
CN1	0.082	0.002	-0.012	0.001
CN2	0.118	0.004	-0.014	0.002
Ca4227	1.101	0.065	0.009	0.033
G4300	5.174	0.115	-0.132	0.061
HgA	-6.013	0.161	0.239	0.079
HgF	-1.370	0.067	0.041	0.033
Fe4383	5.563	0.184	-0.213	0.092
Ca4455	1.247	0.045	-0.097	0.024
Fe4531	3.500	0.118	-0.051	0.058
C4668	8.302	0.229	-0.818	0.121
Hbeta	1.844	0.064	-0.044	0.033
Fe5015	3.857	0.308	-0.069	0.153
Mg1	0.149	0.004	-0.006	0.002
Mg2	0.293	0.0023	-0.012	0.001
Mgb	4.561	0.074	-0.143	0.038
Fe5270	3.0222	0.091	-0.107	0.047
Fe5335	2.750	0.101	-0.073	0.052

Table A.3. Linear fit parameters (Y=a+bx) in the bulge region of NGC 1433

Index	a	err a	b	err b
HdA	0.084	0.210	0.295	0.057
HdF	1.188	0.117	0.171	0.032
CN1	0.067	0.004	-0.008	0.001
CN2	0.093	0.005	-0.007	0.001
Ca4227	0.771	0.038	-0.017	0.010
G4300	4.00	0.103	-0.099	0.028
HgA	-3.378	0.148	0.307	0.045
HgF	-0.165	0.066	0.197	0.023
Fe4383	4.531	0.126	-0.149	0.035
Ca4455	1.077	0.036	-0.020	0.010
Fe4531	3.169	0.048	-0.127	0.016
Fe4668	6.374	0.128	-0.161	0.035
Hbeta	2.059	0.075	0.062	0.021
Fe5015	5.601	0.136	-0.074	0.036
Mg1	0.083	0.002	0.004	0.001
Mg2	0.208	0.002	0.004	0.001
Mgb	2.921	0.071	-0.029	0.018
Fe5270	2.741	0.064	-0.008	0.017
Fe5335	2.613	0.072	-0.088	0.019

Table A.4. Linear fit parameters (Y=a+bx) in the bulge region of NGC 1530

Index	a	err a	b	err b
HdA	2.173	0.210	0.229	0.095
HdF	2.251	0.189	0.105	0.086
CN1	-0.044	0.006	-0.005	0.003
CN2	-0.010	0.007	-0.004	0.003
Ca4227	0.548	0.081	-0.073	0.037
G4300	2.666	0.151	-0.290	0.068
HgA	-1.030	0.441	0.594	0.202
HgF	1.395	0.195	0.223	0.092
Fe4383	3.488	0.301	-0.251	0.140
Ca4455	0.892	0.074	-0.004	0.036
Fe4531	2.049	0.395	-0.123	0.184
Fe4668	6.299	0.242	-0.814	0.115
Hbeta	3.297	0.209	0.084	0.112
Fe5015	5.232	0.255	-0.748	0.124
Mg1	0.076	0.002	-0.007	0.001
Mg2	0.186	0.006	-0.021	0.003
Mgb	2.732	0.166	-0.197	0.079
Fe5270	2.613	0.091	-0.319	0.044
Fe5335	2.501	0.070	-0.321	0.035

Table A.5. Linear fit parameters (Y=a+bx) in the bulge region of NGC 1832

Index	a	err a	b	err b
HdA	3.966	0.226	-1.000	0.131
HdF	3.322	0.168	-0.536	0.096
CN1	-0.081	0.004	0.018	0.002
CN2	-0.047	0.005	0.016	0.003
Ca4227	0.610	0.073	0.059	0.040
G4300	1.769	0.247	0.642	0.130
HgA	1.700	0.436	-1.281	0.242
HgF	2.815	0.238	-0.737	0.131
Fe4383	2.490	0.222	0.4223	0.114
Ca4455	0.792	0.064	0.042	0.034
Fe4531	2.432	0.168	0.133	0.086
C4668	4.478	0.240	0.108	0.120
Hbeta	4.025	0.150	-0.382	0.074
Fe5015	4.398	0.212	0.101	0.106
Mg1	0.044	0.002	0.004	0.001
Mg2	0.1340	0.005	0.009	0.002
Mgb	2.148	0.092	0.206	0.048
Fe5270	2.247	0.101	0.046	0.051
Fe5335	2.058	0.090	0.056	0.045

Table A.6. Linear fit parameters (Y=a+bx) in the bulge region of NGC 2217

Index	a	err a	b	err b
HdA	-3.350	0.123	0.100	0.048
HdF	-0.399	0.057	0.006	0.023
CN1	0.203	0.004	-0.010	0.002
CN2	0.234	0.004	-0.010	0.002
Ca4227	1.260	0.030	0.015	0.013
G4300	5.542	0.071	-0.034	0.029
HgA	-8.555	0.123	0.308	0.050
HgF	-2.994	0.075	0.159	0.030
Fe4383	6.391	0.161	-0.045	0.067
Ca4455	1.282	0.060	0.005	0.025
Fe4531	3.551	0.137	-0.010	0.057
C4668	9.621	0.160	-0.372	0.066
Hbeta	2.093	0.079	-0.141	0.032
Fe5015	6.554	0.117	0.018	0.048
Mg1	0.165	0.002	0.005	0.001
Mg2	0.334	0.002	0.004	0.001
Mgb	5.651	0.057	-0.194	0.023
Fe5270	3.178	0.086	0.075	0.034
Fe5335	3.197	0.064	-0.067	0.026

Table A.7. Linear fit parameters (Y=a+bx) in the bulge region of NGC 2273

Index	a	err a	b	err b
HdA	4.650	0.338	-0.567	0.215
HdF	3.604	0.197	-0.285	0.125
CN1	-0.071	0.008	0.006	0.004
CN2	-0.035	0.008	0.005	0.005
Ca4227	0.271	0.047	0.095	0.031
G4300	1.456	0.210	0.343	0.126
HgA	1.813	0.424	-0.656	0.254
HgF	2.565	0.262	-0.315	0.155
Fe4383	2.4027	0.166	0.384	0.098
Ca4455	0.405	0.063	0.120	0.037
Fe4531	2.292	0.173	0.032	0.098
C4668	3.129	0.246	0.057	0.135
Hbeta	2.930	0.191	0.012	0.096
Fe5015	-0.448	0.588	1.139	0.296
Mg1	0.101	0.008	-0.011	0.003
Mg2	0.141	0.006	0.006	0.002
Mgb	2.150	0.099	0.143	0.056
Fe5270	1.716	0.089	0.169	0.048
Fe5335	1.909	0.081	0.060	0.043

Table A.8. Linear fit parameters (Y=a+bx) in the bulge region of NGC 2523

Index	a	err a	b	err b
HdA	-1.350	0.205	0.052	0.055
HdF	0.588	0.106	0.040	0.029
CN1	0.029	0.006	-0.003	0.002
CN2	0.058	0.006	-0.002	0.002
Ca4227	1.158	0.073	-0.013	0.020
G4300	5.034	0.129	-0.072	0.035
HgA	-4.973	0.187	0.072	0.049
HgF	-0.870	0.076	0.032	0.020
Fe4383	4.684	0.134	0.114	0.034
Ca4455	0.914	0.089	0.049	0.022
Fe4531	3.104	0.133	0.023	0.033
C4668	6.484	0.286	-0.017	0.070
Hbeta	1.918	0.087	0.007	0.021
Fe5015	5.203	0.183	-0.028	0.044
Mg1	0.087	0.003	-0.000	0.001
Mg2	0.227	0.003	-0.001	0.001
Mgb	3.825	0.085	-0.040	0.021
Fe5270	2.870	0.090	-0.038	0.022
Fe5335	2.581	0.100	-0.031	0.024

Table A.9. Linear fit parameters (Y=a+bx) in the bulge region of NGC 2665

Index	a	err a	b	err b
HdA	3.632	0.243	-0.062	0.095
HdF	2.590	0.197	0.059	0.077
CN1	-0.027	0.005	0.002	0.002
CN2	-0.012	0.006	0.006	0.002
Ca4227	0.289	0.044	0.022	0.017
G4300	0.850	0.140	0.318	0.055
HgA	2.402	0.283	-0.421	0.113
HgF	2.647	0.180	-0.216	0.071
Fe4383	2.010	0.248	0.159	0.097
Ca4455	0.397	0.095	0.075	0.037
Fe4531	1.417	0.101	0.146	0.040
C4668	2.514	0.217	0.259	0.083
Hbeta	3.728	0.153	-0.246	0.056
Fe5015	2.998	0.120	0.115	0.047
Mg1	0.0426	0.006	0.011	0.002
Mg2	0.107	0.006	0.016	0.002
Mgb	2.079	0.085	0.034	0.032
Fe5270	1.503	0.097	0.123	0.035
Fe5335	1.448	0.122	0.079	0.043

Table A.11. Linear fit parameters (Y=a+bx) in the bulge region of NGC 2859

Index	a	err a	b	err b
HdA	-2.297	0.105	0.147	0.042
HdF	0.214	0.073	0.057	0.030
CN1	0.094	0.002	-0.009	0.001
CN2	0.128	0.003	-0.010	0.001
Ca4227	1.087	0.027	-0.019	0.011
G4300	5.426	0.090	-0.0588	0.038
HgA	-6.286	0.127	0.163	0.049
HgF	-1.579	0.054	0.042	0.021
Fe4383	5.583	0.099	-0.178	0.040
Ca4455	1.327	0.034	-0.022	0.014
Fe4531	3.450	0.078	-0.077	0.032
C4668	7.345	0.109	-0.221	0.043
Hbeta	2.000	0.047	-0.022	0.019
Fe5015	5.918	0.090	-0.159	0.035
Mg1	0.121	0.003	-0.004	0.001
Mg2	0.274	0.002	-0.006	0.001
Mgb	4.252	0.039	-0.052	0.016
Fe5270	3.070	0.0411	-0.032	0.017
Fe5335	2.916	0.037	-0.082	0.015

Table A.10. Linear fit parameters (Y=a+bx) in the bulge region of NGC 2681

Index	a	err a	b	err b
HdA	5.205	0.102	-0.390	0.048
HdF	3.830	0.062	-0.202	0.030
CN1	-0.082	0.002	0.003	0.001
CN2	-0.0439	0.002	0.003	0.001
Ca4227	0.617	0.019	-0.006	0.010
G4300	1.922	0.065	0.196	0.034
HgA	2.535	0.102	-0.446	0.051
HgF	3.289	0.045	-0.243	0.024
Fe4383	2.736	0.075	-0.009	0.036
Ca4455	0.851	0.020	-0.014	0.010
Fe4531	2.931	0.041	-0.067	0.021
C4668	4.825	0.0806	-0.214	0.041
Hbeta	4.230	0.040	-0.190	0.021
Fe5015	5.504	0.076	-0.211	0.038
Mg1	0.034	0.002	-0.001	0.001
Mg2	0.133	0.002	-0.001	0.001
Mgb	2.204	0.022	-0.028	0.012
Fe5270	2.386	0.039	-0.047	0.020
Fe5335	2.294	0.021	-0.101	0.012

Table A.12. Linear fit parameters (Y=a+bx) in the bulge region of NGC 2935

Index	a	err a	b	err b
HdA	1.001	0.228	0.092	0.080
HdF	1.411	0.123	0.104	0.043
CN1	0.045	0.005	-0.004	0.002
CN2	0.069	0.005	-0.002	0.002
Ca4227	0.705	0.053	-0.009	0.018
G4300	3.402	0.119	-0.048	0.044
HgA	-2.848	0.295	0.207	0.104
HgF	-0.128	0.184	0.145	0.065
Fe4383	4.245	0.112	-0.143	0.041
Ca4455	1.009	0.064	-0.055	0.023
Fe4531	2.725	0.089	-0.067	0.034
C4668	5.757	0.172	-0.248	0.063
Hbeta	2.196	0.089	-0.017	0.032
Fe5015	5.622	0.210	-0.209	0.073
Mg1	0.080	0.003	0.006	0.001
Mg2	0.199	0.004	0.005	0.001
Mgb	2.807	0.141	-0.051	0.049
Fe5270	2.632	0.122	-0.052	0.042
Fe5335	2.243	0.097	-0.010	0.034

Table A.13. Linear fit parameters (Y=a+bx) in the bulge region of NGC 2950

Index	a	err a	b	err b
HdA	-1.959	0.074	0.178	0.024
HdF	0.397	0.036	0.052	0.012
CN1	0.112	0.005	-0.015	0.001
CN2	0.149	0.005	-0.016	0.001
Ca4227	0.967	0.029	-0.009	0.010
G4300	5.091	0.067	-0.051	0.024
HgA	-5.495	0.061	0.126	0.020
HgF	-1.193	0.027	0.053	0.009
Fe4383	5.336	0.061	-0.147	0.021
Ca4455	1.430	0.038	-0.061	0.013
Fe4531	3.559	0.054	-0.087	0.019
C4668	9.607	0.175	-0.662	0.059
Hbeta	2.150	0.031	-0.007	0.011
Fe5015	6.422	0.070	-0.263	0.025
Mg1	0.121	0.002	-0.005	0.001
Mg2	0.272	0.003	-0.009	0.001
Mgb	4.199	0.038	-0.122	0.013
Fe5270	3.271	0.049	-0.109	0.017
Fe5335	3.055	0.055	-0.103	0.019

Table A.15. Linear fit parameters (Y=a+bx) in the bulge region of NGC 3081

Index	a	err a	b	err b
HdA	-4.618	0.232	0.994	0.103
HdF	-2.286	0.164	0.632	0.072
CN1	0.214	0.007	-0.034	0.003
CN2	0.214	0.007	-0.029	0.003
Ca4227	0.121	0.140	0.190	0.065
G4300	1.446	1.056	0.922	0.512
HgA	-2.770	1.726	-0.799	0.765
HgF	-3.906	0.120	0.893	0.055
Fe4383	8.173	0.179	-1.012	0.100
Ca4455	0.525	0.108	0.150	0.055
Fe4531	3.132	0.375	-0.135	0.184
C4668	4.697	0.301	0.212	0.148
Hbeta	0.233	0.181	0.308	0.076
Fe5015	0.233	0.181	0.308	0.076
Mg1	0.293	0.023	-0.044	0.009
Mg2	0.357	0.010	-0.028	0.005
Mgb	3.993	0.096	-0.340	0.052
Fe5270	2.927	0.102	-0.071	0.051
Fe5335	3.083	0.096	-0.229	0.049

Table A.14. Linear fit parameters (Y=a+bx) in the bulge region of NGC 2962

Index	a	err a	b	err b
HdA	-3.122	0.126	0.405	0.067
HdF	-0.068	0.076	0.111	0.039
CN1	0.138	0.005	-0.026	0.002
CN2	0.173	0.006	-0.028	0.003
Ca4227	1.308	0.056	-0.053	0.030
G4300	5.264	0.109	0.056	0.057
HgA	-6.730	0.134	0.176	0.068
HgF	-1.920	0.093	0.093	0.048
Fe4383	5.969	0.1076	-0.303	0.057
Ca4455	1.575	0.058	-0.128	0.030
Fe4531	3.738	0.102	-0.186	0.052
C4668	8.918	0.221	-0.655	0.113
Hbeta	1.615	0.057	0.072	0.029
Fe5015	6.271	0.143	-0.321	0.073
Mg1	0.146	0.003	-0.009	0.001
Mg2	0.314	0.003	-0.017	0.001
Mgb	4.895	0.055	-0.228	0.029
Fe5270	3.373	0.076	-0.128	0.040
Fe5335	3.258	0.074	-0.127	0.041

Table A.16. Linear fit parameters (Y=a+bx) in the bulge region of NGC 4245

Index	a	err a	b	err b
HdA	-3.068	0.184	0.928	0.072
HdF	-0.1189	0.079	0.439	0.031
CN1	0.095	0.006	-0.026	0.002
CN2	0.130	0.005	-0.029	0.002
Ca4227	1.369	0.055	-0.103	0.022
G4300	5.493	0.149	-0.460	0.06
HgA	-6.673	0.236	0.969	0.091
HgF	-1.642	0.135	0.489	0.052
Fe4383	5.936	0.153	-0.393	0.062
Ca4455	1.498	0.057	-0.083	0.023
Fe4531	3.608	0.112	-0.143	0.046
C4668	8.931	0.217	-0.823	0.089
Hbeta	1.973	0.072	0.121	0.029
Fe5015	6.406	0.152	-0.469	0.062
Mg1	0.118	0.003	-0.011	0.001
Mg2	0.280	0.004	-0.021	0.001
Mgb	4.444	0.059	-0.302	0.024
Fe5270	3.445	0.074	-0.176	0.031
Fe5335	3.327	0.150	-0.145	0.061

Table A.17. Linear fit parameters (Y=a+bx) in the bulge region of NGC 4314

Index	a	err a	b	err b
HdA	-3.065	0.162	0.733	0.042
HdF	-0.078	0.104	0.310	0.027
CN1	0.085	0.003	-0.020	0.001
CN2	0.118	0.004	-0.021	0.001
Ca4227	1.462	0.041	-0.125	0.012
G4300	5.706	0.194	-0.491	0.057
HgA	-7.428	0.300	1.027	0.081
HgF	-2.046	0.165	0.506	0.046
Fe4383	6.378	0.162	-0.514	0.050
Ca4455	1.490	0.060	-0.105	0.019
Fe4531	3.651	0.130	-0.200	0.040
C4668	7.769	0.213	-0.593	0.067
Hbeta	1.786	0.075	0.091	0.027
Fe5015	6.143	0.150	-0.367	0.048
Mg1	0.122	0.002	-0.010	0.001
Mg2	0.289	0.004	-0.020	0.001
Mgb	4.541	0.097	-0.265	0.031
Fe5270	3.276	0.086	-0.133	0.030
Fe5335	3.134	0.089	-0.171	0.029

Table A.19. Linear fit parameters (Y=a+bx) in the bulge region of NGC 5101

Index	a	err a	b	err b
HdA	-3.675	0.146	0.173	0.048
HdF	-0.393	0.053	0.059	0.017
CN1	0.178	0.003	-0.008	0.001
CN2	0.209	0.004	-0.008	0.001
Ca4227	1.1481	0.052	-0.013	0.018
G4300	5.586	0.052	-0.039	0.018
HgA	-7.671	0.075	0.137	0.025
HgF	-2.466	0.063	0.059	0.021
Fe4383	6.326	0.120	-0.170	0.042
Ca4455	1.394	0.046	-0.021	0.016
Fe4531	3.446	0.087	-0.031	0.030
C4668	8.434	0.098	-0.202	0.034
Hbeta	1.891	0.053	-0.107	0.019
Fe5015	6.762	0.146	-0.182	0.051
Mg1	0.139	0.001	0.005	0.001
Mg2	0.308	0.002	0.003	0.001
Mgb	4.168	0.087	-0.041	0.030
Fe5270	3.331	0.059	-0.038	0.020
Fe5335	3.069	0.062	-0.075	0.022

Table A.18. Linear fit parameters (Y=a+bx) in the bulge region of NGC 4394

Index	a	err a	b	err b
HdA	-1.694	0.167	0.985	0.072
HdF	0.580	0.116	0.451	0.050
CN1	0.051	0.004	-0.027	0.002
CN2	0.084	0.004	-0.028	0.002
Ca4227	1.017	0.036	-0.041	0.016
G4300	5.051	0.114	-0.440	0.054
HgA	-5.368	0.230	1.102	0.105
HgF;	-1.051	0.109	0.547	0.050
Fe4383	5.381	0.098	-0.482	0.044
Ca4455	1.404	0.049	-0.150	0.023
Fe4531	3.557	0.070	-0.228	0.033
C4668	7.653	0.142	-0.851	0.068
Hbeta	2.214	0.069	0.161	0.031
Fe5015	5.530	0.124	-0.202	0.058
Mg1	0.090	0.004	-0.010	0.001
Mg2	0.238	0.004	-0.017	0.001
Mgb	3.918	0.077	-0.276	0.036
Fe5270	3.216	0.059	-0.210	0.028
Fe5335	2.953	0.070	-0.200	0.033